PAPER

Check for updates

Efficient narrowband electroluminescence based on a hetero-bichromophore thermally activated delayed fluorescence dyad†

You-Jun Yu,‡[a] Sheng-Nan Zou,‡[a] Chen-Chen Peng,[a] Zi-Qi Feng,[a] Yang-Kun Qu, [ID][a] Sheng-Yi Yang,[a] Zuo-Quan Jiang [ID] *[a] and Liang-Sheng Liao [ID] *[ab]

A hetero-bichromophore thermally activated delayed fluorescence (TADF) emitter named **BOQAO** was designed and synthesized, which consists of two multi-resonance TADF (MR-TADF) cores, *t*BuBO and *t*BuQAO. The short-range intramolecular charge transfer (ICT) characteristics of *t*BuBO and *t*BuQAO weaken its electron-donating and electron-withdrawing ability, respectively. Thus, weak long-range ICT from *t*BuBO to *t*BuQAO is established in **BOQAO** for holding blue fluorescence emission with a slight redshift, keeping a small FWHM, and maintaining the TADF properties, simultaneously. The simple doped devices exhibited high color purity with FWHMs of less than 35 nm in a wide doping ratio range from 1 wt% to 40 wt%. At a 5 wt% doping ratio, the device based on **BOQAO** exhibited the best device performance with an EQE of 21.8% and an FWHM of 32 nm. This work provides a simple and practical strategy for suppressing aggregation-induced spectral broadening for the development of MR-TADF.

Introduction

Commercial organic light-emitting diode (OLED) technology requires a high device efficiency, good color purity, and a long device lifetime simultaneously.[1–5] In the past decade, thermally activated delayed fluorescence (TADF) OLEDs have already demonstrated their potential as the third generation of OLEDs due to their 100% exciton utilization and low cost. In a TADF molecule, the small energy splitting between the lowest excited singlet (S_1) and triplet (T_1) states, ΔE_{ST}, provides a practical pathway for harvesting non-emissive triplet excitons through the spin-flipping reverse intersystem crossing (RISC) process.[6,7] To achieve an effective RISC process, the general strategy is to reduce the exchange energy between the highest occupied molecular orbital (HOMO) and the lowest unoccupied molecular orbital (LUMO) by constructing a donor–acceptor (D–A) type emitter with a twisted structure.[8–11] However, the subsequent conformation relaxation caused by the twisted structures usually enhances the structure relaxation and leads to a wide emission with a full-width at half maximum (FWHM) of >70 nm, which is unsuitable for commercial displays.[12]

To withstand the broadened FWHM of conventional D–A-type TADF emitters, Hatakeyama *et al.* proposed the multi-resonance (MR) TADF emitter named DABNA-1, which exhibited a pure blue emission centered at 459 nm with an external quantum efficiency (EQE) of 13.5% and an impressively small FWHM of 28 nm.[13] For DABNA-1, the *ortho*-positioned boron and nitrogen atoms lead to the multi-resonance effect for facilitating the RISC process; meanwhile, the rigid planar polycyclic aromatic framework ensures the narrow emission. Hereafter, TADF emitters with a narrow FWHM were widely studied and more chromophores with the MR effect were developed.[14–21] Among them, oxygen-bridged triarylboranes have also been exploited as narrowband emitters, and the parent molecule DABOA[14] (2a) exhibited a narrow emission (FWHM = 34 nm) with a λ_{PL} of 398 nm in solution.[22] In 2019, our group disclosed another successful example, QAO, which bears MR-TADF activity aside from the prevalent B/N or B/O system, which consisted of a triphenylamine having two *para*-disposed carbonyl bridges, and its electroluminescent device achieved an EQE of 19.4% with a narrow FWHM of 39 nm.[23] This result provides a promising candidate for the design of highly efficient and narrowband organic emitters.

Although the above-mentioned MR-TADF cores improve the color purity immensely with FWHMs of less than 40 nm, their

[a] *Institute of Functional Nano & Soft Materials (FUNSOM), Jiangsu Key Laboratory for Carbon-Based Functional Materials & Devices, Soochow University, 199 Ren'ai Road, Suzhou, 215123, Jiangsu, P. R. China. E-mail: zqjiang@suda.edu.cn, lsliao@suda.edu.cn*

[b] *Macau Institute of Materials Science and Engineering, Macau University of Science and Technology, Macau 999078, P. R. China*

‡ These authors contributed equally.

This journal is © The Royal Society of Chemistry 2022

J. Mater. Chem. C, 2022, **10**, 4941–4946 | **4941**

RISC rates are still limited, which is caused by the same π–$\pi^{\star}$ transition characteristic for both S_1 and T_1 states.[24] The introduction of general electron donors (arylamines) or acceptors has proven an effective strategy, which creates a long-range intramolecular charge transfer (ICT) state for improving the device efficiency and tuning the bandgap.[25–44] This strategy usually improved the color purity due to the vanished shoulder peak. However, such modification for blue MR-TADF emitters usually enhanced the structural relaxation, broadened the emission spectra, and redshifted the emission band. For instance, the introduction of 9,9-dimethyl-9,10-dihydroacridine (DMAC) at the QAO core caused a large dihedral angle and a wide emission band (FWHM > 70 nm).[23] Moreover, the utilization of a conventional electron donor with moderate steric hindrance (*i.e.*, carbazole) could also virtually decrease the color purity (FWHM ≈ 50 nm).[33] Thus, the introduction of a weak ICT state could be a practical pathway to develop blue MR-TADF emitters.

Herein, we combined two MR-TADF cores (*t*BuBO and *t*BuQAO) to construct a hetero-bichromophore dyad named **BOQAO**. The difference in electron-donating and electron-withdrawing ability of the MR segments drives a long-range ICT interaction, where *t*BuBO and *t*BuQAO serve as an electron-donor and electron-acceptor, respectively. Compared with the emission peak of *t*BuQAO in dilute toluene solution, the slight redshift (7 nm) of **BOQAO** indicates weak long-range ICT. In doped 4,4′-bis(*N*-carbazolyl)-1,1′-biphenyl (CBP) films with wide doping ratios (1–30 wt%), **BOQAO** exhibits high color purity with small FWHMs of less than 40 nm. The doped devices also suggest high color purity within a wide doping ratio range (1–40 wt%). At a 5 wt% doping ratio, the device based on **BOQAO** exhibited the best device performance with an EQE of 21.8% and an FWHM of 32 nm.

Results and discussion

Synthesis and characterization

The synthetic route for **BOQAO** is summarized in Scheme 1. For 2,5-dibromo-1,3-dimethylbenzene (**1**), the dimethyl group can be easily converted to the diester *via* an oxidation and esterification reaction.[45] After the Ullmann reaction, hydrolysis, and the Friedel–Crafts acylation reaction, the bromine-containing *t*BuQAO segment (**6**) can be obtained. After the Miyaura borylation reaction, intermediate **7** was obtained with a high yield (84%). The target compound **BOQAO** was obtained *via* the Suzuki–Miyaura coupling reaction with an oxygen-bridged triarylborane scaffold (**8**). The characterization results are presented in Fig. S12–S16 (ESI†). The newly reported compounds were characterized using ^{1}H-NMR, ^{13}C-NMR, and mass spectra. We also evaluate the thermal stability of **BOQAO** *via* thermogravimetric analysis (TGA) and differential scanning calorimetry (DSC). As shown in Fig. S1 (ESI†), the high decomposition temperature (T_d, corresponding to a 5% weight loss) of 485 °C suggest its outstanding thermal stability.[46–48] No obvious glass transition temperature (T_g) was found in the DSC curve.
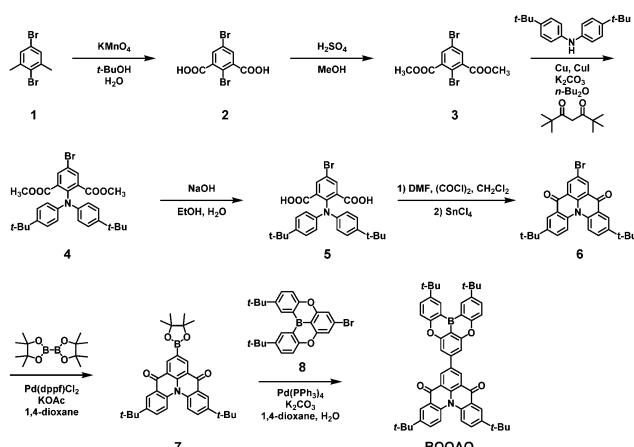
Single crystal

As shown in Fig. 1 and Table S3 (ESI†), the single crystal was obtained *via* the slow liquid diffusion of petroleum ether in a dichloromethane solution of **BOQAO** at room temperature. The *t*BuQAO segment exhibits a twisted helicene structure with a dihedral angle of 43.6° between the terminal phenyl rings, and the *t*BuBO fragment maintains a relatively planar structure with a dihedral angle of 13.4° between the corresponding phenyl rings. In addition, the dyad maintains a torsion angle of 33.7° between the *t*BuBO and *t*BuQAO moieties. The dumbbell-shaped structure of **BOQAO** leads to a mixed parallel H-aggregate and J-aggregate packing.[49] In detail, the bulky *tert*-butyl groups and different helicene-shaped *t*BuBO and *t*BuQAO moieties cause a relatively large distance of 3.31 Å for the H-aggregate dimer and a short distance of 3.19 Å between the adjacent J-aggregate dimers, respectively. Such a packing mode makes **BOQAO** maintain high intermolecular restrictions, which is favorable for high fluorescence efficiency in the aggregation states.

Simulation and electrochemical properties

Density functional theory (DFT) and time-dependent DFT (TD-DFT) were employed to evaluate the molecular configurations and orbitals (Fig. S2 in the ESI†). The highest occupied molecular orbital (HOMO) and the lowest unoccupied molecular orbital (LUMO) of **BOQAO** are located at the *t*BuBO and *t*BuQAO segments, respectively. Such well-separated frontier molecular

Scheme 1 Synthetic route for **BOQAO**.
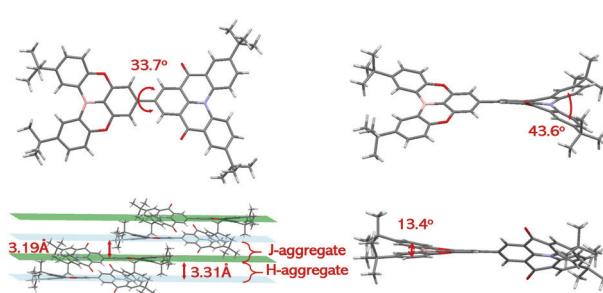
Fig. 1 Single crystal structure and packing mode of **BOQAO**.

4942 | *J. Mater. Chem. C*, 2022, **10**, 4941–4946

This journal is © The Royal Society of Chemistry 2022
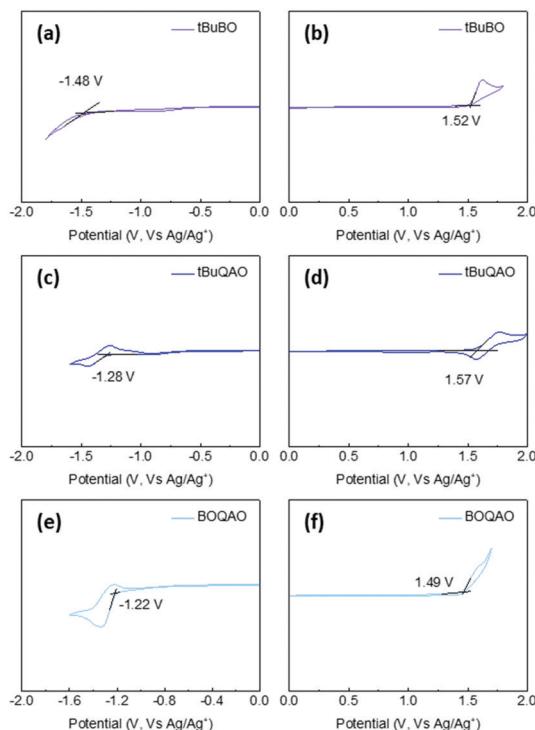
Fig. 2 Cyclic voltammetry (CV) curves of (a and b) *t*BuBO, (c and d) *t*BuQAO, and (e and f) **BOQAO**.

Fig. 3 Photophysical properties of **BOQAO**. (a) Absorption and fluorescence spectra of **BOQAO** in dilute toluene solution (10^{-5} mol L^{-1}) at room temperature. (b) Fluorescence spectra of **BOQAO** in different solutions. (c) Fluorescence spectra of **BOQAO** in doped CBP films. (d) Transient spectra of 5 wt% **BOQAO** in CBP at different temperatures.

orbitals (FMOs) feed the requirement for typical D–A-type TADF emitters with a small ΔE_{ST}, which also indicated that ICT from *t*BuBO to *t*BuQAO could occur for fluorescence emission.[50] Furthermore, **BOQAO** exhibits a small structural relaxation, which is supported by the calculated S_0 and S_1 geometries.[51] Besides, the dipole moment of **BOQAO** of the S_0 state is as small as 3.017 Debye, which is favorable for suppressing the redshift caused by intermolecular interactions.

Furthermore, the energy levels of **BOQAO** were evaluated through cyclic voltammetry (CV) measurements (Fig. 2). The quasi-reversible oxidation and irreversible reduction potentials of **BOQAO** are 1.49 and −1.22 V, respectively. Furthermore, the corresponding HOMO and LUMO energy levels of **BOQAO** are calculated to be −5.77 and −3.06 eV, respectively. The bandgap for **BOQAO** is 2.71 eV. The wide bandgap suggests that **BOQAO** would still maintain blue fluorescence. The CV curves of the parents *t*BuBO and *t*BuQAO were also measured for comparison (Fig. 2). Evaluating the positions and curve shapes, the *t*BuBO and *t*BuQAO moieties in **BOQAO** serve as electron-donor and -acceptor, respectively, which agrees with the calculated HOMO and LUMO distributions.[46,48]

Photophysical properties

The photophysical properties of **BOQAO** and their parent segments *t*BuBO and *t*BuQAO were investigated simultaneously in solution (Fig. 3 and Fig. S5–S7 in the ESI†). In degassed dilute toluene solution, **BOQAO** exhibits a blue emission peak maximum at 474 nm and an FWHM of 28 nm. Compared with the fluorescence spectra of *t*BuQAO (Fig. S5c, ESI,† peak at 467 nm

and an FWHM of 29 nm), the slight redshift (7 nm) indicates that the long-range ICT from *t*BuBO to *t*BuQAO is weak and the electron-donating ability of *t*BuBO and the electron-withdrawing ability *t*BuQAO in **BOQAO** are weakened by the short-range ICT of the segments. The symmetrical absorption and fluorescence spectra with small FWHM values suggest the strong low-frequency vibronic coupling in this system.[52] Furthermore, the small Stokes shift of 925 cm^{-1} indicates that the dyad still maintained a small reorganization energy between the ground and excited conformations, which is consistent with the small configuration difference between the S_0 and S_1 states (Fig. S2 in the ESI†).[51] Compared with the absorption band at 300–400 nm (corresponding to the higher excited state), the lower intensity of the lowest absorption band (centered at 455 nm, corresponding to the lowest excited state) indicates that the long-range ICT does work.[53] Furthermore, the lowest absorption band of **BOQAO** is slightly redshifted but maintains a MR-type shape compared with the absorption band of the parents *t*BuBO and *t*BuQAO (Fig. S5 in the ESI†), which indicates that the weak long-range ICT interactions between the two MR segments does not have a significant influence on the FWHM.[54] The fluorescence spectra in different polar solvents were also investigated (Fig. 3b and Fig. S6, Table S1 in the ESI†). An obvious redshift and broadened spectra can be observed. For instance, **BOQAO** exhibits a blue emission with a peak at 456 nm and an FWHM of 24 nm in cyclohexane solution and a sky-blue emission with a peak at 484 nm and an FWHM of 38 nm in dichloromethane solution. To evaluate the S_1 and T_1 energy levels, we also measured the fluorescence and phosphorescence spectra of **BOQAO** and its parent segments *t*BuBO and *t*BuQAO in toluene at 77 K (Fig. S7 in the ESI†). The calculated S_1 and T_1 energy levels of **BOQAO** are 2.68 and 2.46 eV, respectively. Thus, the **BOQAO** maintains a relatively small ΔE_{ST} of 0.22 eV, which is comparable to *t*BuBO (ΔE_{ST} = 0.19 eV) and

This journal is © The Royal Society of Chemistry 2022

J. Mater. Chem. C, 2022, **10**, 4941–4946 | **4943**
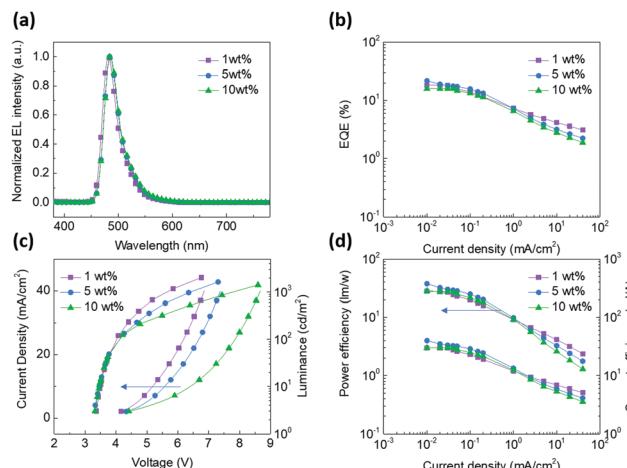
Fig. 4 OLED device performance for **BOQAO**. (a) Normalized electroluminescence spectrum. (b) EQE–current density curves. (c) Current density–voltage–luminescence curves. (d) Power efficiency–current density–current efficiency curves.

*t*BuQAO (ΔE_{ST} = 0.22 eV), to support the RISC process for triplet exciton utilization. The triplet spin density of **BOQAO** (Fig. S3 in the ESI†) indicates that the *t*BuBO segment partly contributes to the triplet excited states.

Moreover, **BOQAO** exhibited narrowband sky-blue emission with a negligible redshift when doped in CBP with the doping ratio increasing from 1 to 30 wt% (Fig. 3c). The emission peaks of **BOQAO** at 1, 5, 10, and 30 wt% in CBP are 483, 487, 489, and 490 nm with FWHMs of 31, 33, 34, and 38 nm, respectively. Such properties are uncommon among MR-TADF emitters, which are a result of low dipolar moment, highly molecular rigidity, and intermolecular restrictions in the aggregation state.[26,55,56] Furthermore, these results also indicate that our strategy can effectively suppress spectral broadening. The TADF characteristics of **BOQAO** were further investigated *via* their fluorescence decay curves at 5 wt% in CBP at different temperatures (Fig. 3d). The prompt and delayed fluorescence lifetimes are 6 ns and 214 μs, respectively. Moreover, the decayed fluorescence exhibits obvious temperature-dependent properties. In addition, the absolute PL quantum yields (PLQY) of the doped films of 5 wt% *t*BuBO, *t*BuQAO, and **BOQAO** in CBP were measured to be 97.0%, 93.1%, and 98.7%, respectively, which indicate that the hetero-bichromophore emitter **BOQAO** exhibited improved the PLQY. The fluorescence decay curves and PLQY values of *t*BuBO and *t*BuQAO doped in CBP films (Fig. S9 and Tables S3, S4 in the ESI†) were also measured to evaluate the kinetics of the excited states. Compared with *t*BuBO and *t*BuQAO, **BOQAO** maintains a comparable singlet radiative transition rate constant (k_r^S = 3.2 × 10^7) and RISC rate constant (k_{RISC} = 2.4 × 10^4). Furthermore, **BOQAO** exhibits less triplet energy loss, which is supported by the small triplet nonradiative rate constant (k_{nr}^T = 7.5 × 10^1).

Electroluminescence properties

To evaluate the device performance, simple doped devices were fabricated with the structure of indium tin oxide (ITO)/1,4,5,8,9,11-hexaazatriphenylene hexacarbonitrile (HAT-CN, 10 nm)/1,1-bis[4-[*N,N*-di(*p*-tolyl)amino]phenyl]-cyclohexane (TAPC, 40 nm)/tris(4-carbazolyl-9-ylphenyl)amine (TCTA, 10 nm)/CBP: *x* wt% **BOQAO** (20 nm)/4,6-bis(3,5-di(pyridin-4-yl)phenyl)-2-phenylpyrimidine (TmPyPB, 45 nm)/8-hydroxyquinolinolato lithium (Liq, 2 nm)/Al (100 nm). TAPC and TmPyPB were chosen as the hole-transporting layer and the electron-transporting layer, respectively, and TCTA was adopted as an exciton-blocking layer for confining excitons due to its high triplet energy level. Fig. S10 (in the ESI†) shows the energy level diagram of the devices and the molecular structures of the related functional materials.

As shown in Fig. 4a, the electroluminescence spectra of all the devices with 1, 5, 10 wt% doping ratios maintain a sky-blue emission with peaks at 484 nm and FWHMs of 32 nm, respectively, which match the fluorescence spectra of the corresponding films. The devices with a higher doping ratio (up to 40 wt%) also maintain impressively small FWHMs in the sky-blue region (Fig. S11 in the ESI†). Among these devices, the device with a 5 wt% doping ratio of **BOQAO** in CBP exhibits the best device performance with a maximum external quantum efficiency (EQE$_{max}$) of 21.8%, which is the best performance among the reported QAO derivatives in the blue region (Table S4 in the ESI†).

Conclusions

In summary, an MR-TADF emitter named **BOQAO**, which consists of two MR segments *t*BuBO and *t*BuQAO, was designed and synthesized. Long-range ICT from *t*BuBO fragment to *t*BuQAO fragment in **BOQAO**, which is weakened by short-range ICT in the segments, was established to tune its photophysical properties. Compared with the parent MR core *t*BuQAO, **BOQAO** exhibits a blue emission (peak at 474 nm and FWHM of 28 nm) with a slightly redshifted emission. In doped CBP films with a wide doping ratio range of 1–30 wt%, **BOQAO** displays a persistent blue emission with small FWHMs of less than 40 nm. This unique property is also demonstrated in the electroluminescence spectra of the doped devices. The optimized device with a 5 wt% doping ratio of **BOQAO** in CBP realized the best device performance with an EQE$_{max}$ of 21.8% and an FWHM of 32 nm, which balanced the color purity and device efficiency. This work provides a practical strategy for suppressing spectral broadening for the development of MR-TADF.

Conflicts of interest

There are no conflicts to declare.

Acknowledgements

4944 | *J. Mater. Chem. C*, 2022, **10**, 4941–4946

This journal is © The Royal Society of Chemistry 2022

References

1 C. W. Tang and S. A. VanSlyke, *Appl. Phys. Lett.*, 1987, **51**, 913–915.

2 P. T. Chou and Y. Chi, *Chem. – Eur. J.*, 2007, **13**, 380–395.

3 Y. Tao, K. Yuan, T. Chen, P. Xu, H. Li, R. Chen, C. Zheng, L. Zhang and W. Huang, *Adv. Mater.*, 2014, **26**, 7931–7958.

4 S. Y. Yang, Y. K. Qu, L. S. Liao, Z. Q. Jiang and S. T. Lee, *Adv. Mater.*, 2021, 2104125, DOI: 10.1002/adma.202104125.

5 M. Romain, D. Tondelier, O. Jeannin, B. Geffroy, J. Rault-Berthelot and C. Poriel, *J. Mater. Chem. C*, 2015, **3**, 9701–9714.

6 Z. Yang, Z. Mao, Z. Xie, Y. Zhang, S. Liu, J. Zhao, J. Xu, Z. Chi and M. P. Aldred, *Chem. Soc. Rev.*, 2017, **46**, 915–1016.

7 H. Uoyama, K. Goushi, K. Shizu, H. Nomura and C. Adachi, *Nature*, 2012, **492**, 234–238.

8 Y.-J. Yu, X.-Q. Wang, J.-F. Liu, Z.-Q. Jiang and L.-S. Liao, *iScience*, 2021, **24**, 102123.

9 Y. J. Yu, X. Tang, H. T. Ge, Y. Yuan, Z. Q. Jiang and L. S. Liao, *Org. Electron.*, 2019, **73**, 240–246.

10 P. Data and Y. Takeda, *Chem. – Asian J.*, 2019, **14**, 1613–1636.

11 M. Y. Zhang, Z. Y. Li, B. Lu, Y. Wang, Y. D. Ma and C. H. Zhao, *Org. Lett.*, 2018, **20**, 6868–6871.

12 P. Data, P. Pander, M. Okazaki, Y. Takeda, S. Minakata and A. P. Monkman, *Angew. Chem., Int. Ed.*, 2016, **55**, 5739–5744.

13 T. Hatakeyama, K. Shiren, K. Nakajima, S. Nomura, S. Nakatsuka, K. Kinoshita, J. Ni, Y. Ono and T. Ikuta, *Adv. Mater.*, 2016, **28**, 2777–2781.

14 D. Hall, S. M. Suresh, P. L. dos Santos, E. Duda, S. Bagnich, A. Pershin, P. Rajamalli, D. B. Cordes, A. M. Z. Slawin, D. Beljonne, A. Köhler, I. D. W. Samuel, Y. Olivier and E. Zysman-Colman, *Adv. Opt. Mater.*, 2019, **8**, 1901627.

15 H. Min, I. S. Park and T. Yasuda, *Angew. Chem., Int. Ed.*, 2021, **60**, 7643–7648.

16 M. Nagata, H. Min, E. Watanabe, H. Fukumoto, Y. Mizuhata, N. Tokitoh, T. Agou and T. Yasuda, *Angew. Chem., Int. Ed.*, 2021, **60**, 20280–20285.

17 G. Liu, H. Sasabe, K. Kumada, A. Matsunaga, H. Katagiri and J. Kido, *J. Mater. Chem. C*, 2021, **9**, 8308–8313.

18 Y. Kondo, K. Yoshiura, S. Kitera, H. Nishi, S. Oda, H. Gotoh, Y. Sasada, M. Yanai and T. Hatakeyama, *Nat. Photonics*, 2019, **13**, 678–682.

19 S. Oda, B. Kawakami, R. Kawasumi, R. Okita and T. Hatakeyama, *Org. Lett.*, 2019, **21**, 9311–9314.

20 Y. Zhang, D. Zhang, J. Wei, Z. Liu, Y. Lu and L. Duan, *Angew. Chem., Int. Ed.*, 2019, **58**, 16912.

21 S. N. Zou, C. C. Peng, S. Y. Yang, Y. K. Qu, Y. J. Yu, X. Chen, Z. Q. Jiang and L. S. Liao, *Org. Lett.*, 2021, **23**, 958–962.

22 H. Hirai, K. Nakajima, S. Nakatsuka, K. Shiren, J. Ni, S. Nomura, T. Ikuta and T. Hatakeyama, *Angew. Chem., Int. Ed.*, 2015, **54**, 13581–13585.

23 Y. Yuan, X. Tang, X.-Y. Du, Y. Hu, Y.-J. Yu, Z.-Q. Jiang, L.-S. Liao and S.-T. Lee, *Adv. Opt. Mater.*, 2019, **7**, 1801536.

24 X. Wu, B.-K. Su, D.-G. Chen, D. Liu, C.-C. Wu, Z.-X. Huang, T.-C. Lin, C.-H. Wu, M. Zhu, E. Y. Li, W.-Y. Hung, W. Zhu and P.-T. Chou, *Nat. Photonics*, 2021, **15**, 780–786.

25 M. Yang, S. Shikita, H. Min, I. S. Park, H. Shibata, N. Amanokura and T. Yasuda, *Angew. Chem., Int. Ed.*, 2021, **60**, 23142.

26 Y. Xu, C. Li, Z. Li, Q. Wang, X. Cai, J. Wei and Y. Wang, *Angew. Chem., Int. Ed.*, 2020, **59**, 17442.

27 X. Liang, Z. P. Yan, H. B. Han, Z. G. Wu, Y. X. Zheng, H. Meng, J. L. Zuo and W. Huang, *Angew. Chem., Int. Ed.*, 2018, **57**, 11316–11320.

28 Y. Liu, X. Xiao, R. You, Z. Bin and J. You, *Chem. Sci.*, 2021, **12**, 9408–9412.

29 M. Yang, I. S. Park and T. Yasuda, *J. Am. Chem. Soc.*, 2020, **142**, 19468–19472.

30 J. U. Kim, I. S. Park, C. Y. Chan, M. Tanaka, Y. Tsuchiya, H. Nakanotani and C. Adachi, *Nat. Commun.*, 2020, **11**, 1765.

31 D. H. Ahn, S. W. Kim, H. Lee, I. J. Ko, D. Karthik, J. Y. Lee and J. H. Kwon, *Nat. Photonics*, 2019, **13**, 540–546.

32 Y. Qi, W. Ning, Y. Zou, X. Cao, S. Gong and C. Yang, *Adv. Funct. Mater.*, 2021, **31**, 2102017.

33 F. Huang, K. Wang, Y. Z. Shi, X. C. Fan, X. Zhang, J. Yu, C. S. Lee and X. H. Zhang, *ACS Appl. Mater. Interfaces*, 2021, **13**, 36089–36097.

34 D. Karthik, Y. H. Jung, H. Lee, S. Hwang, B. M. Seo, J. Y. Kim, C. W. Han and J. H. Kwon, *Adv. Mater.*, 2021, **33**, 2007724.

35 H. Lim, H. J. Cheon, S. J. Woo, S. K. Kwon, Y. H. Kim and J. J. Kim, *Adv. Mater.*, 2020, **32**, 2004083.

36 Y. Xu, Q. Wang, X. Cai, C. Li and Y. Wang, *Adv. Mater.*, 2021, **33**, 2100652.

37 R. Braveenth, H. Lee, J. D. Park, K. J. Yang, S. J. Hwang, K. R. Naveen, R. Lampande and J. H. Kwon, *Adv. Funct. Mater.*, 2021, **31**, 2105805.

38 Y. Lee and J. I. Hong, *Adv. Opt. Mater.*, 2021, **9**, 2100406.

39 X. F. Luo, F. L. Li, J. W. Zou, Q. Zou, J. Su, M. X. Mao and Y. X. Zheng, *Adv. Opt. Mater.*, 2021, **9**, 2100784.

40 I. S. Park, H. Min, J. U. Kim and T. Yasuda, *Adv. Opt. Mater.*, 2021, **9**, 2101282.

41 C. Wu, W. Liu, K. Li, G. Cheng, J. Xiong, T. Teng, C. M. Che and C. Yang, *Angew. Chem., Int. Ed.*, 2021, **60**, 3994–3998.

42 M. Yang, S. Shikita, H. Min, I. S. Park, H. Shibata, N. Amanokura and T. Yasuda, *Angew. Chem., Int. Ed.*, 2021, **60**, 23142–23147.

43 Y. Chen, N. Li, Z. Huang, G. Xie and C. Yang, *Chem. Eng. J.*, 2022, **430**, 133078.

44 J. Hwang, H. Kang, J.-E. Jeong, H. Y. Woo, M. J. Cho, S. Park and D. H. Choi, *Chem. Eng. J.*, 2021, **416**, 129185.

45 S. K. Surampudi, G. Nagarjuna, D. Okamoto, P. D. Chaudhuri and D. Venkataraman, *J. Org. Chem.*, 2012, **77**, 2074–2079.

46 L. Sicard, C. Quinton, F. Lucas, O. Jeannin, J. Rault-Berthelot and C. Poriel, *J. Phys. Chem. C*, 2019, **123**, 19094–19104.

47 H. Yang, Q. Liang, C. Han, J. Zhang and H. Xu, *Adv. Mater.*, 2017, **29**, 1700553.

This journal is © The Royal Society of Chemistry 2022

J. Mater. Chem. C, 2022, **10**, 4941–4946 | **4945**

48 M. Romain, D. Tondelier, B. Geffroy, A. Shirinskaya, O. Jeannin, J. Rault-Berthelot and C. Poriel, *Chem. Commun.*, 2015, **51**, 1313–1315.

49 N. J. Hestand and F. C. Spano, *Chem. Rev.*, 2018, **118**, 7069–7163.

50 Y. C. Liu, C. S. Li, Z. J. Ren, S. K. Yan and M. R. Bryce, *Nat. Rev. Mater.*, 2018, **3**, 18020.

51 Y. Zhang, D. Zhang, T. Huang, A. J. Gillett, Y. Liu, D. Hu, L. Cui, Z. Bin, G. Li, J. Wei and L. Duan, *Angew. Chem., Int. Ed.*, 2021, **60**, 20498.

52 X. Qiu, G. Tian, C. Lin, Y. Pan, X. Ye, B. Wang, D. Ma, D. Hu, Y. Luo and Y. Ma, *Adv. Opt. Mater.*, 2021, **9**, 2001845.

53 S. Y. Yang, S. N. Zou, F. C. Kong, X. J. Liao, Y. K. Qu, Z. Q. Feng, Y. X. Zheng, Z. Q. Jiang and L. S. Liao, *Chem. Commun.*, 2021, **57**, 11041–11044.

54 X. C. Fan, K. Wang, Y. Z. Shi, J. X. Chen, F. Huang, H. Wang, Y. N. Hu, Y. Tsuchiya, X. M. Ou, J. Yu, C. Adachi and X. H. Zhang, *Adv. Opt. Mater.*, 2021, **10**, 2101789.

55 Y. Zhang, J. Wei, D. Zhang, C. Yin, G. Li, Z. Liu, X. Jia, J. Qiao and L. Duan, *Angew. Chem., Int. Ed.*, 2021, **61**, e202113206.

56 P. Jiang, J. Miao, X. Cao, H. Xia, K. Pan, T. Hua, X. Lv, Z. Huang, Y. Zou and C. Yang, *Adv. Mater.*, 2021, 2106954, DOI: 10.1002/adma.202106954.